LIMNOLOGY
and
OCEANOGRAPHY

ASLO

Limnol. Oceanogr. 65, 2020, 2125–2141

doi: 10.1002/lno.11443

Return of the "age of dinoflagellates" in Monterey Bay: Drivers of dinoflagellate dominance examined using automated imaging flow cytometry and long-term time series analysis

Alexis D. Fischer ,* **Kendra Hayashi, Anna McGaraghan, Raphael M. Kudela**
Ocean Sciences Department, University of California Santa Cruz, Santa Cruz, California

Abstract

Phytoplankton biomass in Monterey Bay, California is typically dominated by diatoms, but it shifted to dinoflagellates twice in the past 18 years (2004–2007, 2017–2018), which was associated with increased harmful algal blooms. Located within the central California Current System (CCS), Monterey Bay is strongly influenced by cycles of upwelling-favorable winds and their relaxation or reversal. Both dinoflagellate-dominated periods were linked to a negative North Pacific Gyre Oscillation (NPGO) and increased river discharge, but each had a different relationship with upwelling. To examine the connection between large-scale and local forcings underlying floristic shifts in the phytoplankton assemblage, an Imaging FlowCytobot (IFCB) was deployed within the Monterey Bay upwelling shadow for a full year. A machine learning classifier differentiating IFCB images of the phytoplankton assemblage was developed. Despite anomalously strong upwelling in 2018, dinoflagellates comprised 57% of the annual phytoplankton-specific biomass. During upwelling, dinoflagellates appear to have accumulated at convergent fronts, while during relaxation these frontal populations were transported to the nearshore where they seeded local blooms. Frequent upwelling-relaxation cycles and local wind anomalies generated an unusually retentive circulation pattern in the upwelling shadow, producing a warm and stratified bloom incubator. Thus, local features and forcings (upwelling shadow, winds, river discharge) modified the effects of regional- and basin-scale oceanographic variability (regional upwelling, NPGO), altering local phytoplankton patterns. As North Pacific decadal variability and CCS upwelling intensity increase under climate warming, dinoflagellates may become more common in some CCS regions, due to the enhancement or mitigation of large-scale trends by local forcings.

Eastern boundary current coastal upwelling systems are among the most biologically productive regions in the global ocean (e.g., Ryther 1969). Seasonal succession of phytoplankton taxa is attributed to variations in wind-driven upwelling, which affects both nutrient supply to the euphotic zone and stratification (Margalef 1978; Garrison 1979; Figueiras and Ríos 1993; Kudela et al. 2005; García-Reyes and Largier 2012). In one such ecosystem, the California Current System (CCS), seasonal upwelling in the spring brings cool, high salinity, nutrient-rich water to the surface, fueling large blooms of chain-forming diatoms and the highest annual primary productivity (e.g., Garrison 1979; García-Reyes and Largier 2012). In the autumn, upwelling-favorable winds relax and the California Current collapses onshore, which results in stratification, lower surface nutrients, and dinoflagellate blooms. During the winter, reduced light availability and increased physical mixing from storms leads to lower phytoplankton biomass. Deviations from this canonical phytoplankton pattern can alter important ecosystem functions, including primary production, biogeochemical cycling (e.g., Cloern 1996), plankton community structure (e.g., Sommer 2002), and energy transfer through the food web (e.g., Platt et al. 2003).

In the past two decades, short-term shifts in the dominant phytoplankton group from diatoms to dinoflagellates have been observed in the CCS (Cloern et al. 2005; White et al. 2014; Du et al. 2015). These changes have been associated with ecological and economic impacts because of increased dinoflagellate harmful algal blooms (HABs). When dinoflagellates dominated the CCS phytoplankton community (Taylor et al. 2015) and base of the food web (Litz et al. 2010) in 2005–2006, zooplankton biomass, forage fish biomass, and seabird fecundity decreased, and marine mammal foraging was altered

*Correspondence: adfische@ucsc.edu

Additional Supporting Information may be found in the online version of this article.

(Peterson et al. 2006; Sydeman et al. 2006; Weise et al. 2006). In Monterey Bay, California, a shift to an anomalous dinoflagellate-dominated system occurred during 2004–2007 (Jessup et al. 2009; Jester et al. 2009*b*; Mazzillo et al. 2011), termed the "age of dinoflagellates" (Chavez 2006). This change was associated with increased paralytic shellfish toxins in sentinel shellfish and finfish (Jester et al. 2009*a*; 2009*b*) and a seabird mortality event in 2007 due to algal surfactant-plumage fouling from a large bloom of the dinoflagellate *Akashiwo sanguinea* (Jessup et al. 2009). Similarly, in 2009, a massive bloom of *A. sanguinea* spanning the Washington and Oregon coasts caused significant seabird mortality (Du et al. 2011; White et al. 2014; Jones et al. 2017). The mechanisms underlying floristic shifts from diatom- to dinoflagellate-dominance in the CCS remain inconclusive thus far (e.g., Jester et al. 2009*b*).

Temporal changes in phytoplankton abundance and community composition in coastal upwelling systems can be attributed to the complex interplay between local features (e.g., upwelling shadow) and forcings (e.g., local winds, local river discharge), and low frequency, basin-scale processes, such as climate oscillations. Climate indices aggregate changing conditions across ocean basins and can reveal multifactor influences on marine populations through shifts in ocean currents, temperature, mixing, and primary productivity (e.g., Peterson and Schwing 2003). For example, dinoflagellate abundance off the Oregon coast increased as the Pacific Decadal Oscillation (PDO) shifted to its positive phase in 2002, and dinoflagellate abundance declined when the PDO shifted to a negative state in 2008 (Du et al. 2015). Temporal shifts in the phytoplankton can also be influenced by the North Pacific Gyre Oscillation (NPGO; Cloern et al. 2010; Sydeman and Thompson 2010) and El Niño Southern Oscillation (ENSO; Venrick 2012). However, few long-term syntheses of phytoplankton community structure have successfully linked deviations from canonical patterns to local environmental variability and large-scale ocean climate variability.

The well-studied Monterey Bay (Fig. 1) presents an opportunity to investigate unusual shifts from diatom to dinoflagellate dominance. Monterey Bay, located in the central CCS, is strongly influenced by wind-driven upwelling that varies seasonally in intensity and intermittency (Pennington and Chavez 2000; Ryan et al. 2011) and is tightly coupled with phytoplankton community transitions (e.g., Ryan et al. 2008, 2014). A long-term phytoplankton and water quality time series (2001–2018) and a recent deployment of an Imaging FlowCytobot (IFCB; Olson and Sosik 2007) at the Santa Cruz Municipal Wharf (SCMW) permit observations of the phytoplankton community at interannual scales (Jester et al. 2009*b*; Lane et al. 2009) and high temporal frequency (hourly), respectively. The IFCB produces high-quality images of individual phytoplankton ($\sim$ 10–150 μm) and an automated machine learning classifier can be constructed to identify the phytoplankton images to the genus-level and sometimes even species-level (e.g., Sosik and Olson 2007).

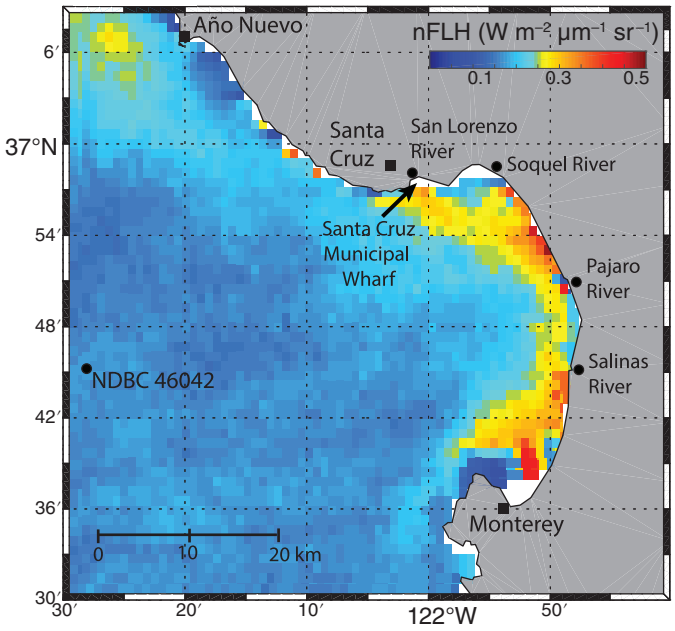

Fig. 1. Map of Monterey Bay, California highlighting the location of the Santa Cruz Municipal Wharf where local samples were collected, the four river mouths, the offshore buoy used for regional wind data (NDBC 46042), and the Año Nuevo upwelling center. The average satellite-observed chlorophyll nFLH for January–March 2018 is shown in the background.

Through the lens of a representative California Current ecosystem, this study mechanistically examines how shifts in nearshore phytoplankton dynamics in Monterey Bay are influenced by both basin-scale and local environmental variability. An 18-yr weekly SCMW time series of phytoplankton abundance, environmental variables, and climate indices were analyzed using a partial least-squares regression (PLSR) model. Two periods of anomalous dinoflagellate dominance (2004–2007, 2017–2018) occurred during this time series and their similarities and differences are discussed. These insights are interpreted in the context of a year of IFCB data documenting fine-scale changes in the phytoplankton community in response to local forcings.

Methods

Study site

Monterey Bay is a highly productive coastal upwelling environment in the central CCS (Fig. 1). Cold filaments originating from the Año Nuevo upwelling center typically flow southward across the bay mouth and bifurcate, such that water flows both offshore and into the bay (Rosenfeld et al. 1994). The combination of this upwelling circulation and coastal geomorphology creates an "upwelling shadow" in the northern bay, where residence time and stratification are enhanced (Graham and Largier 1997). Within these sheltered waters, phytoplankton thrive on episodic nutrient supply and can form dense blooms,

which can rapidly spread throughout the bay (e.g., Ryan et al. 2008).

In the upwelling shadow at the SCMW (36.96°N, 122.02°W), there is a long-term data set of physical, chemical, and biological water properties from regular sampling, initially as part of the California Program for Regional Enhanced Monitoring for PhycoToxins (Cal-PReEMPT, 2000–2006), and later as part of the Central and Northern California Ocean Observing System (CeNCOOS, 2007–2018). The shore station is located midway down the SCMW (330 m from land), and the water below is typically well mixed and shallow (mean water depth = 8 m).

Weekly water sampling at the SCMW

Discrete water samples were collected approximately weekly from 2001 through 2018 at the SCMW. During 2001 to mid-2006, only surface-water samples were collected, but after mid-2006, water was collected from three depths (0, 1.5, and 3 m) and combined to create a depth-integrated sample representative of the upper water column. Sea surface temperature (SST) was measured immediately following sample retrieval using a calibrated thermometer. Sample water for nutrient analysis was filtered through ~ 0.7 μm Whatman GF/F filters into polyethylene bottles and frozen pending analysis. Nitrate plus nitrite (hereafter referred to as "nitrate") was analyzed using a Lachat QuikChem 8500 Flow Injection Analyst System and Omnion 3.0 software. Chlorophyll *a* (Chl *a*) samples were collected on ~ 0.7 μm Whatman GF/F filters, extracted for 24 h in 90% acetone (–20°C), and analyzed using the nonacidification technique (Welschmeyer 1994) on a Turner Designs 10-AU fluorometer calibrated with pure Chl *a*.

The longest running time series of phytoplankton community composition at the SCMW is the Relative Abundance Index (RAI) dataset. Approximately weekly, a vertical net tow sample was collected using a 20 μm mesh net towed through the upper 3 m of the water column 5× following standard methods employed by the California Department of Public Health monitoring program (https://www.cdph.ca.gov/Programs/CEH/DRSEM/Pages/EMB/Shellfish/Annual-Mussel-Quarantine.aspx). The final volume was reduced to approximately 300 mL and the live sample was viewed under a dissecting microscope (Leica 10Z125) at 64× magnification. A semiquantitative analysis of phytoplankton cell abundance was made using a ranking system of visually estimated biovolume: "absent" (no cells); "present" (1–10% of the biomass); "common" (11–50%); "abundant" (> 50%) (Curtiss et al. 2008; Jester et al. 2009*b*). Because the phytoplankton biomass varied between samples, the percentage composition data for taxa of interest was normalized by calculating a RAI. For each sample, the percent composition of individual taxa was summed and then individual taxa values were adjusted so that the total percent composition was equal to 100%. This data set was used to represent dinoflagellates in statistical analyses. To account for differences in biomass across the time series, the adjusted RAI values corresponding to only dinoflagellate taxa were summed and multiplied by the Chl *a* concentration (hereafter referred to as "dinoflagellate chlorophyll" or "dinoflagellate Chl *a*").

Environmental data

Local meteorological, hydrological, and climatological data were obtained from various sources to investigate drivers of dinoflagellate abundance (Table 1). To assess the impact of regional upwelling, Bakun Upwelling Index data (Bakun 1973) for the Monterey Bay region were downloaded and regional wind forcing data were obtained from the National Data Buoy Center (NDBC) (Fig. 1) and rotated to upwelling favorable winds (i.e., equatorward and parallel to the regional coastline). Local wind data from SCMW were obtained and local surface current forcing was evaluated with high-frequency radar (HFr) data. To assess water column stratification, Regional Ocean Modeling System (ROMS) temperature data for the nearest grid point were obtained from the ROMS Monterey Nowcast system. Local discharge rates were downloaded from the United States Geological Survey. Three Pacific basin indices forced by changes in large-scale patterns of atmospheric variability were downloaded: the NPGO, Multivariate ENSO Index Version 2 (MEI.v2), and PDO. The NPGO captures the dominant decadal scale fluctuations of salinity and nutrients in the central and eastern North Pacific (Di Lorenzo et al. 2008, 2009). The MEI is an indicator of ENSO activity (Wolter and Timlin 2011) and positive values indicate El Niño conditions. To spatially examine bloom development, chlorophyll normalized fluorescence line height (nFLH = FLH normalized to solar geometry to account for seasonality) and SST images from the MODIS multispectral sensor on the Aqua satellite (https://oceancolor.gsfc.nasa.gov/) were used. MODIS data were processed from Level 2 data files using the NASA standard processing package (SeaDAS), applying calibrations developed by the NASA Ocean Biology Processing Group.

Partial least-squares regression

To discover the key environmental variables that drive dinoflagellate chlorophyll anomalies in the northern Monterey Bay, a PLSR was used. The inherent limitations of traditional multivariate regression approaches in handling multi-collinear and noisy data, such as this study's 18-yr time series, can be overcome by applying techniques based on multivariate statistical projection, such as PLSR (Carrascal et al. 2009). PLSR is a recent technique that combines features from the principal component analysis (PCA) technique and the multiple linear regression technique and generalizes them (Abdi 2010). PLSR assumes the dependency between variables and estimates the underlying structures, which are essentially linear combinations of the original variables (Carrascal et al. 2009; Singh et al. 2013). Schulien et al. (2017) also applied PLSR to identify the environmental variables most aligned with phytoplankton blooms in the same SCMW data set; thus, we selected the same method for consistency.

Table 1. Source and measurement frequency of the variables used in analyses. All data are from the Santa Cruz Municipal Wharf unless specified.

Type of data	Frequency	Variable	Units	Source
Biological	25 min	Phytoplankton taxa abundance	cells mL^{-1}	Imaging FlowCytobot
		Phytoplankton-specific carbon	carbon μg mL^{-1}	Imaging FlowCytobot
		Relative Abundance Index	Relative fraction of biomass	Net tow sample counted via microscopy
		Chl *a*	μg L^{-1}	Water sample analyzed using a 10-AU turner fluorometer
Meteorological	15 min	Wind speed and direction	cm s^{-1}, degrees	WeatherHawk 610-series weather station
		Regional wind speed and direction (NDBC buoy 46042)		https://www.ndbc.noaa.gov/station_page.php?station=46042&unit=E
Hydrological	Weekly	Sea surface nitrate	μmol L^{-1}	Water sample analyzed using a Lachat QuikChem 8000 Series
		Sea surface temperature	°C	Water sample measured with a calibrated thermometer
	Daily	Bakun upwelling index (36°N, 122°W)	m^3 s^{-1}	https://oceanwatch.pfeg.noaa.gov/products/PFELData/upwell/daily/p10dayac.all
	Hourly	Sea surface currents (mean of 12 vectors from 36.92–36.97°N and 122.04–121.93°W)	m s^{-1}	http://hfrnet.ucsd.edu/thredds/catalog.html
	6 h	Vertical temperature profile (ROMS: 36.92°N, 122.05°W)	°C	http://legacy.cencoos.org/thredds/catalog.html
	15 min	Discharge rate (San Lorenzo River)	ft^3 s^{-1}	https://waterdata.usgs.gov/ca/nwis/uv?site_no=11161000
Climatological	Monthly	Multivariate ENSO Index Version 2	—	https://www.esrl.noaa.gov/psd/enso/mei/data/meiv2.data
		North Pacific Gyre Oscillation	—	http://www.o3d.org/npgo/npgo.php
		Pacific Decadal Oscillation	—	http://research.jisao.washington.edu/pdo/PDO.latest.txt

Prior to PLSR analysis, dinoflagellate chlorophyll and river discharge were log-transformed, and all variables were standardized to reduce heteroscedasticity. In order to not emphasize seasonal signals, nonseasonal anomalies were calculated for dinoflagellate chlorophyll and all environmental variables (excluding the climatological indices) as in Pennington and Chavez (2017). First, a mean annual cycle was created by binning the raw 18-yr time series into 14-d bins for each calendar year, then averaging each bin's contents to produce a climatological year. Next, the raw time series was gridded into the same 14-d bins for the 18-yr time series using a Stineman (1980) interpolation and smoothed with a 9-point moving average, to de-emphasize short-term variability. Finally, seasonality was removed by taking subtracting the mean annual cycle from the smoothed time series. Monthly climatological indices were also interpolated onto the same 14-d bins to match the nonseasonal anomaly time series.

PLSR was used to determine the relationship between the predictor matrix $X_{m\times n}$, which consists of m variables and n timepoints (environmental data), and a response vector $y_{n\times 1}$ (dinoflagellate chlorophyll). Similar to PCA, PLSR strives to identify a few linear combinations (components) of the original x-values that describe most of the inherent variable information in y. In contrast to PCA, only the most important linear combinations are used in the regression equation in PLSR, which is achieved mathematically by maximizing the covariance between y and all possible linear functions of x. Cross-validation was used to determine the number of significant PLSR components and which environmental variables should be included. The final PLSR models had the lowest root-mean-squared error-of-prediction vs. component number and the greatest percent of variance explained by each component. Thus, the predictability of the model was maximized while the error was minimized. River discharge, surface nitrate, the Upwelling Index, NPGO, MEI, local winds, and SST anomalies were all statistically important predictive variables and were therefore included in final PLSR models. Mixed layer depth (stratification), local surface currents, and the PDO were also evaluated in the PLSR models, but were not statistically significant and were excluded from the final models.

IFCB shore station

High temporal frequency phytoplankton community composition data were acquired with an IFCB, an imaging-in-flow cytometer that captures high quality images of phytoplankton at rates of up to 12 s^{-1}. The IFCB was developed by Olson and Sosik (2007) and is now commercially available from McLane Research Laboratories (Falmouth, MA). The IFCB was secured on a platform above the SCMW sampling site and a peristaltic pump (Stenner Pump Company) was used to vertically pump seawater through 5 m of opaque PVC tubing (1/8″ inner diameter). The tubing intake was set to 2 m below the mean tide level and the mean tidal range was approximately 1 m. The water below the wharf is well mixed, so IFCB samples would approximate discrete water samples collected for microscopy. To maintain the physical integrity of phytoplankton, the lowest possible pump speed was used and the IFCB sampled the seawater before it entered the pump.

The IFCB collects and images an approximately 5 mL seawater sample every 25 min and is capable of operating continuously. For the 2018 time series examined in this study, there are several gaps (usually 1 d, maximum 9 d) due to electrical power failures caused by storms or for maintenance. Before entering the IFCB, seawater passes through a 1 mm copper mesh shroud on the PVC tubing intake to prevent biofouling and a 130 μm Nitex screen to prevent clogging of the IFCB's flow cell. The Nitex screen and the camera field of view set the effective upper size limit of cells, chains, or colonies seen in these images to length ~ 300 μm. The triggering mechanism (scattering vs. fluorescence) affects the lower size limit of cells. For the fluorescence triggering used in this study, the lower size limit was set by the minimum fluorescence intensity needed to trigger the camera and the pixel size of the camera. For the settings at the SCMW, cells larger than 10 μm typically had strong enough fluorescence intensities to trigger images that were visually informative.

Phytoplankton image classifier development

Development of a Monterey Bay-specific phytoplankton image classifier was undertaken using a suite of publicly available MATLAB-based tools (https://github.com/hsosik/ifcb-analysis/). An early version of this software was described by Sosik and Olson (2007) and subsequent development has led to numerous improvements, including replacement of the original support vector machine with a random forest algorithm (Breiman 2001). Using this random forest machine-classification scheme, an image's features (e.g., image dimensions, geometry, cell shape, texture) are compared to those from training image sets defining species, genus, and group-specific plankton classes.

Example images of over 95 species and genus-level categories were manually identified through an iterative process that reviewed IFCB images collected during sampling from September 2016 to August 2019. For the final classifier version used in this analysis, 24 classes were selected that best represented the phytoplankton community composition of the study area. To ensure even distribution of training data across classes, at least 500 and no more than 5000 images for each class were included in the training set. The classifier included 13 classes of diatoms, 10 classes of dinoflagellates, and the class nanoplankton (cells < 10 μm that could not be taxonomically identified from the images). Due to difficulties distinguishing single cells of *Pseudo-nitzschia* spp. from other pennate diatoms, the final "*Pseudo-nitzschia*" class only includes chains—thus single cells of the genera *Pseudo-nitzschia* would be auto-classified as "Unidentified pennate diatoms." The performance of the classifier for specific phytoplankton taxa was assessed for sensitivity (the ability to detect a select class) and precision (the ability of the classifier to discriminate between a select class and other organisms):

$$\text{Sensitivity} = \frac{\text{TP}}{\text{TP} + \text{FN}}$$

$$\text{Precision} = \frac{\text{TP}}{\text{TP} + \text{FP}}$$

where TP, FP, TN, and FN were the number of true positive, false positive, true negative, and false negative images

Table 2. Sensitivity and precision for each of the 24 phytoplankton classes during application of the random forest classification scheme to the image test set.

	Sensitivity	Precision
Akashiwo sanguinea	0.98	0.96
Alexandrium	0.74	0.89
Amylax, *Gonyaulax*, and *Protoceratium*	0.75	0.81
Asterionellopsis	0.89	0.90
Unidentified centric diatoms	0.89	0.89
Ceratium	0.99	0.98
Chaetoceros	0.92	0.86
Margalefidinium	0.94	0.92
Unidentified nanoplankton	0.97	0.98
Cylindrotheca and *Nitzschia*	0.95	0.94
Detonula, *Cerataulina*, and *Lauderia*	0.92	0.91
Dictyocha	0.91	0.92
Dinophysis	0.97	0.93
Eucampia	0.90	0.93
Guinardia and *Dactyliosolen*	0.83	0.93
Gymnodinium	0.92	0.90
Lingulodinium	0.95	0.92
Unidentified pennate diatoms	0.90	0.95
Prorocentrum	0.97	0.97
Pseudo-nitzschia	0.98	0.97
Scrippsiella and *Heterocapsa*	0.96	0.91
Skeletonema	0.90	0.94
Thalassionema	0.84	0.99
Thalassiosira	0.90	0.95

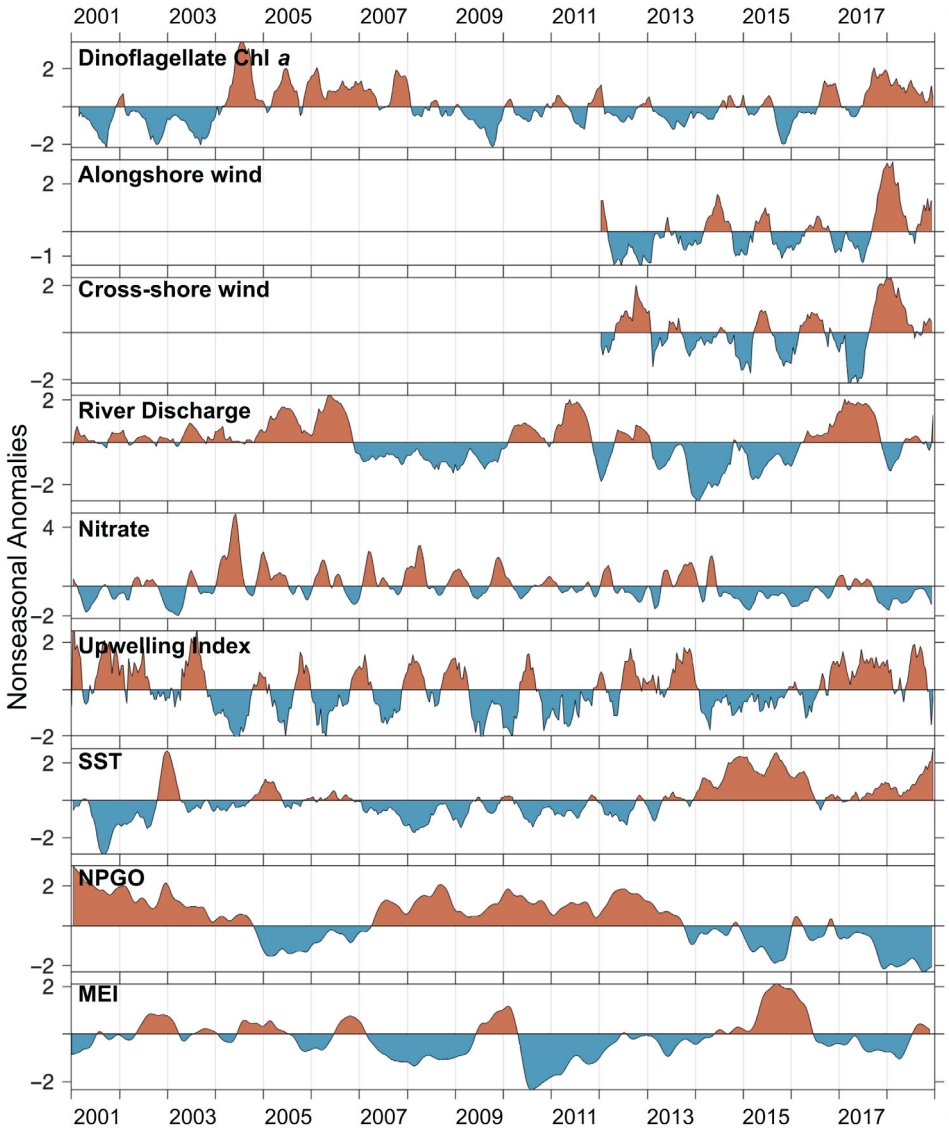

Fig. 2. Long-term physical and chemical context for dinoflagellate shifts at the SCMW from 2001 through 2018. Panels show nonseasonal anomalies (*y*-axis) of dinoflagellate Chl *a*, alongshore wind (positive = eastward/into the bay), cross-shore wind (positive = northward), river discharge, surface nitrate concentration, Upwelling Index, SST, and phases of the NPGO and MEI. Dinoflagellate Chl *a* and river discharge data are log-transformed. Nonseasonal anomalies are shown in the units standard deviations from the seasonal mean.

according to whether they were correctly classified as a member of a class, or not. Precision was extremely high, with the 24 classes used in this analysis having an average score of 0.93 (SE = 0.01) (Table 2). Sensitivity was also high and classes had an average score of 0.90 (SE = 0.01). Only 5% of the images taken in 2018 were unable to be identified by our classifier. The absolute abundances of cells (or chains) in these samples were determined from their apparent abundance by correcting the nominally 5 mL volume sampled to reflect the actual volume of seawater observed by the IFCB, which was always slightly less than 5 mL volume due to a short "dead time" following each trigger during which time each image is processed and stored. The morphometrics of each cell or chain were also used to determine phytoplankton biovolumes from the two-dimensional outlines in each image, using a distance map method (Moberg and Sosik 2012). Images of fluorescent microspheres of a known diameter (9 μm, Duke Scientific) were collected to provide the pixel-to-micron factor necessary to calibrate these estimated biovolumes in μm^3. Phytoplankton biovolume was then converted into units of carbon (pg carbon particle^{-1}) with the volume-to-carbon relationships described by Menden-Deuer and Lessard (2000), which include a correction factor for large diatom taxa. No significant differences in carbon-to-volume relationship among taxa were found, except in the case of large diatoms

(> 3000 μm^3), which had lower carbon content presumably due to the presence of intracellular vacuoles (Menden-Deuer and Lessard 2000).

To assess consistencies across different methodologies, a daily averages of IFCB measurements were compared to weekly SCMW time series estimates of Chl *a* and phytoplankton abundance from corresponding sampling days. In addition to RAI metrics, phytoplankton in whole water samples were enumerated quantitively via the Utermöhl method and fluorescence in situ hybridization for comparison (Supporting Information Fig. S1, Table S1). For a detailed discussion of IFCB method comparisons, see Supporting Information.

Results

Interannual drivers of anomalous dinoflagellate abundance

Dinoflagellates were anomalously abundant from February 2004 through 2007 and September 2017 through 2018 at the SCMW (Fig. 2). A PLSR model using river discharge, surface nitrate, SST, NPGO, and MEI anomalies could predict 30% of dinoflagellate chlorophyll anomalies from 2001 through 2018. To evaluate the individual drivers of each dinoflagellate-dominated period and include the effects of local wind (available from 2012 onward), separate PLSR models for 2001–2011 and 2012–2018 were constructed and component weights for their respective PLSR models were examined. Weights describe how strongly each PLSR component depends on the original variables, and in what direction.

The 2001–2011 PLSR model, which included the Upwelling Index, river discharge, SST, surface nitrate, NPGO, and MEI anomalies, could account for 35% of the dinoflagellate chlorophyll variance annually. Component 1 could predict 31% of the variance and its major weight was a negative NPGO and its associated effects: reduced upwelling and warm SSTs (Fig. 3). These factors lead to water column stratification, which is typically favorable to dinoflagellate growth (Margalef 1978). Increased river discharge and surface nitrate were also present as weights and the latter was likely a result of the former. Component 2 (4% of the variance) included a strongly negative MEI and its associated effects of reduced SST and reduced precipitation in northern California (Hoell et al. 2015), evident by negative river discharge and surface nitrate weights. A negative NPGO and its associated weight of reduced upwelling was also present in Component 2.

The 2012–2018 model included the same environmental variables as the 2001–2011 model, with the exception of the Upwelling Index and the addition of local winds (Fig. 3). It could predict 62% of anomalous dinoflagellate chlorophyll annually (Supporting Information Fig. S2). The major weights in Component 1 (58% of the variance) were anomalous northward and eastward local winds, which would have contributed toward retentive conditions in the northern Monterey Bay (Fig. 3). Also present was a negative NPGO and its associated weights of reduced surface nitrate and increased SST, in addition to a negative MEI weight and positive river discharge. The presence of both negative NPGO and MEI weights, which are associated with weakened and strengthened upwelling, respectively, may have canceled out the effects of the Upwelling Index in the 2012–2018 model. The dominant weights in Component 2 (4% of the variance) were increased river discharge and a negative MEI. Notably, when only the months January through May were analyzed, the PLSR model could explain 74% of anomalous dinoflagellate chlorophyll (Supporting Information Fig. S2). Local alongshore and cross-shore winds were the most influential variables in the 2012–2018 model, accounting for 33% of dinoflagellate chlorophyll anomalies annually, and for 54% during just January–May.

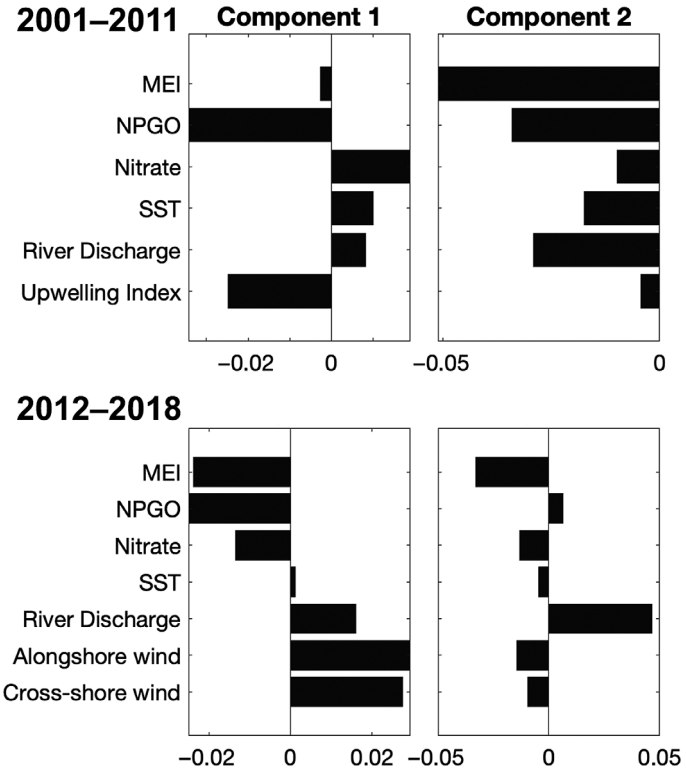

Fig. 3. Positive and negative weights associated with each component in the PLSR models for 2001–2011 and 2012–2018 to predict dinoflagellate anomalies at the SCMW. Local alongshore wind (positive = eastward/into the bay); local cross-shore wind (positive = northward).

Local drivers of phytoplankton community shifts in 2018

The drivers of the 2017–2018 dinoflagellate proliferation in the northern Monterey Bay were resolved in finer detail with continuous daily phytoplankton observations from the IFCB (Fig. 4a). In 2018, the total phytoplankton-specific carbon biomass was 57% dinoflagellates, while diatoms comprised 40%, and nanoplankton comprised 3%. In the typically low-biomass season of January–March, a bloom (detected with MODIS nFLH images) covered a large extent of northern and

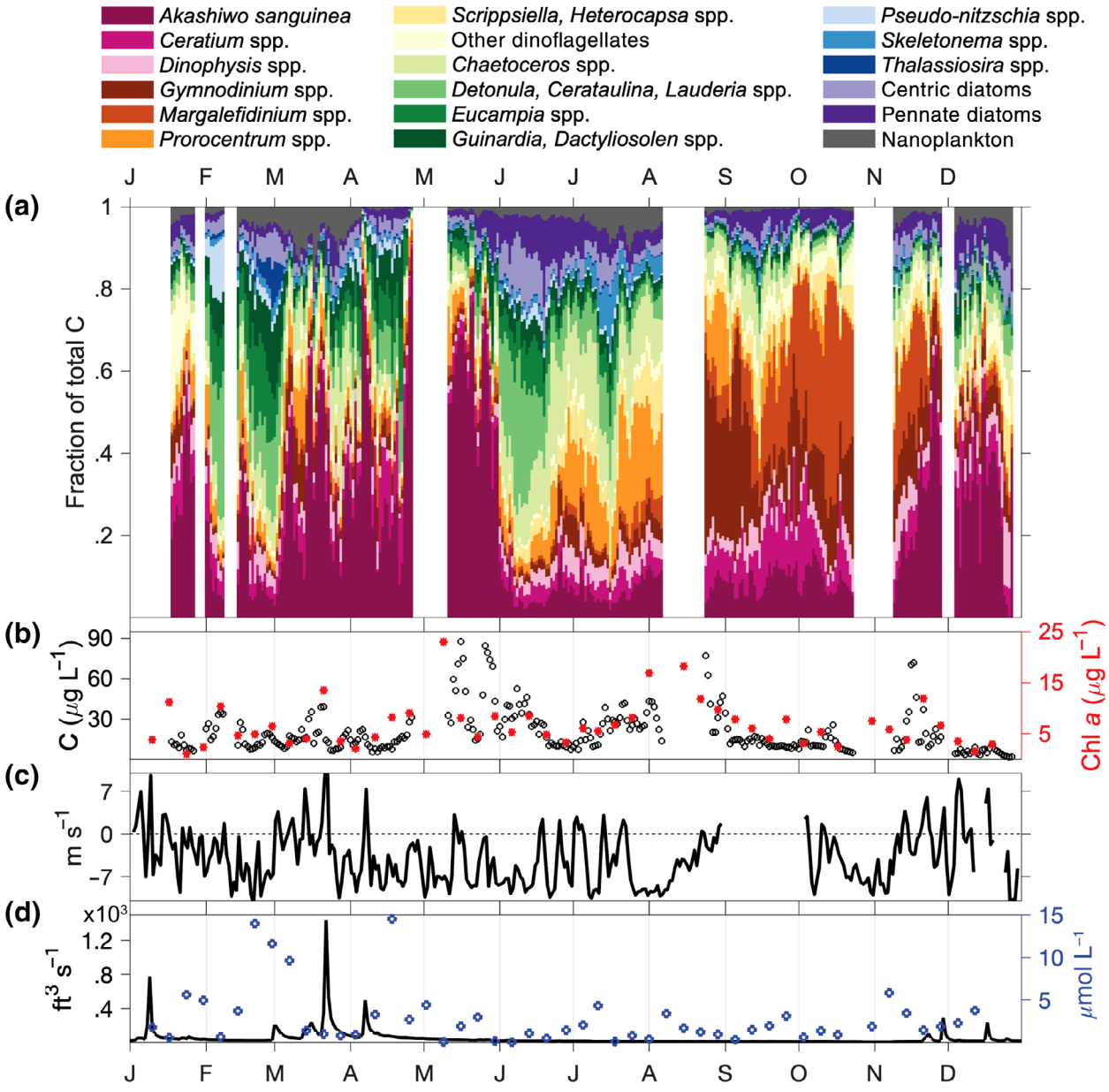

Fig. 4. (**a**) Daily IFCB time series of phytoplankton-specific carbon fractions of dinoflagellate taxa (pinks, reds, oranges, yellows), diatom taxa (greens, blues, purples), and nanoplankton (gray) at the SCMW in 2018. White bands indicate data gaps. (**b**) Concentration of daily IFCB-derived phytoplankton carbon biomass (**c**) in comparison to weekly samples of extracted Chl *a*. (**c**) Alongshore wind speed from regional NDBC buoy 46042 (negative equatorward/upwelling favorable). (**d**) San Lorenzo river discharge and SCMW nitrate concentrations.

southern Monterey Bay (Fig. 1) and dinoflagellates comprised 54% of that biomass in the northern bay (Fig. 4a). Dinoflagellates also encompassed an unusually high percentage (75%) of the phytoplankton-specific carbon biomass in April and May. This anomalous abundance of dinoflagellates was fueled by exceptional environmental conditions.

Frequent upwelling-relaxation cycles characterized the Monterey Bay in 2018. Regional winds at NDBC buoy 46042 were upwelling-favorable for several weeks and then interspersed with several days of reduced wind speed and direction reversal (Fig. 4c). Local winds at the SCMW were weak (rarely exceeding 3 m s^{-1}) and blew predominantly eastward and northward (Supporting Information Fig. S3). These upwelling relaxation/reversal periods, in conjunction with retentive local circulation, produced warm SSTs and stratified conditions in the northern bay. Several examples of large dinoflagellate blooms developing under these conditions throughout the year are described next.

In the winter, strong upwelling (17–27 February) followed by an extended period of relaxation and wind reversal (01–20 March) coincided with the shift from a diatom- to dinoflagellate-dominated community (Figs. 4a, 5a). On 20 February, cold upwelled water from the Año Nuevo upwelling center that had traveled down the coast entered the warm northern bay (Fig. 6a), resulting in nitrate concentrations increasing from 3 to 14 μmol L^{-1} at the SCMW (Fig. 4d). During this time, phytoplankton biomass (as visualized by nFLH MODIS imagery) was low and dispersed. On 23 February, cold upwelled water continued to enter the northern bay and began to set up a thermal front where it encountered the warm, upwelling shadow water, also evident in the surface current divergence in the north central bay (Fig. 6b). Phytoplankton were retained in the northern bay, while the southern bay water mass began to be advected out of the bay. The resulting warm surface temperatures and upwelled nutrients in the northern bay likely helped fuel phytoplankton growth. On 25 February, upwelling filament thermal fronts became more defined and the northern bay phytoplankton bloom intensified (Fig. 6c). Southward currents caused the northern bay bloom to spread down the coast to the central bay, while the southern bay bloom continued to be advected out of the bay. By 27 February, upwelled water had cooled most of the bay (Fig. 6d) and nitrate concentrations at the SCMW continued to be elevated (12 μmol L^{-1}) (Fig. 4d). Strong frontal thermal gradients continue to retain the northern bay bloom, while the southern bay bloom was nearly completely advected from the bay. During this upwelling period, the nearshore phytoplankton community at the SCMW was dominated by the diatom generas *Chaetoceros*, *Detonula*, *Ceratulina*, *Lauderia*, *Eucampia*, *Guinardia*, and *Dactyliosolen*, and had a background population of dinoflagellates (Fig. 4a). However, when regional winds reversed and relaxed on 01 March, dinoflagellates became the dominant taxa.

During the reversal/relaxation period from 01 to 15 March, the water mass at the SCMW became warmer and stratified (Fig. 5d). This northern bay water mass was retained by local surface currents shifting frequently from westward to eastward (Fig. 5c)—perhaps due to residual thermal gradients from February's upwelling. Westward currents from 01 to 03 March began to drive the water mass out of the bay, but eastward currents from 05 to 08 March reversed this pattern, and the process was repeated by subsequent westward (09–12 March) and eastward currents (12–15 March). This retention of warm

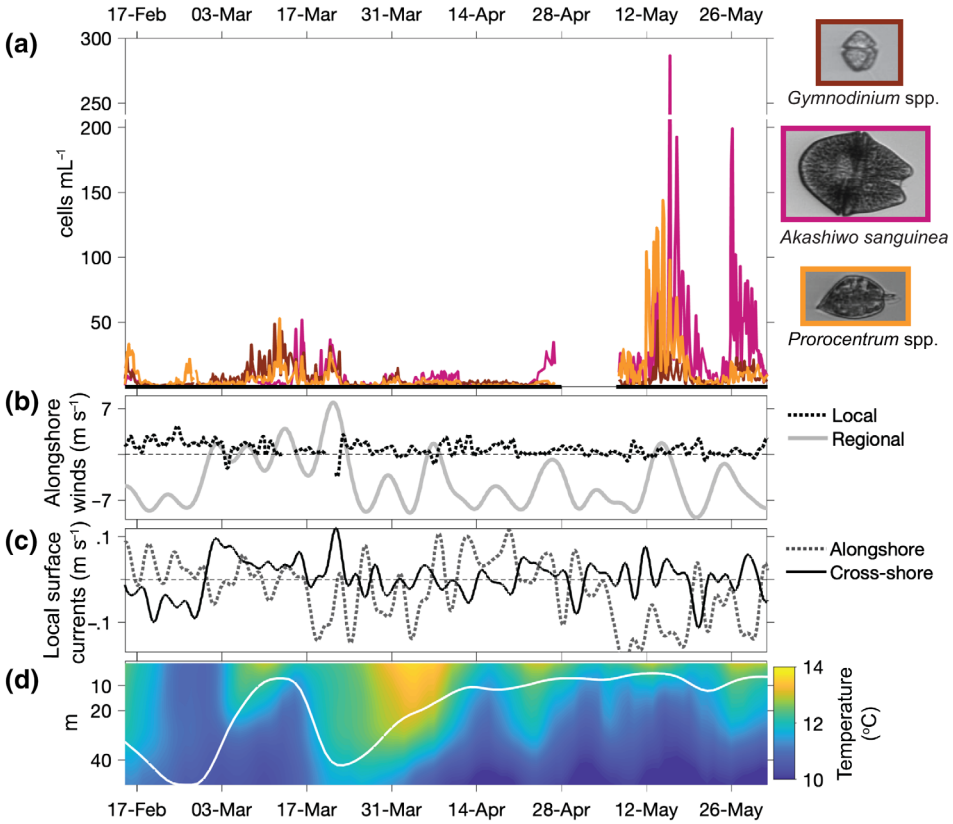

Fig. 5. High resolution (4 h) time series from 17 February through 28 May 2018 at the SCMW of the (**a**) dominant dinoflagellate taxa cell concentrations, (**b**) alongshore wind speed from NDBC buoy 46042 (negative equatorward/upwelling favorable) and local alongshore wind speed (positive eastward/into the bay), (**c**) alongshore surface current speed (positive eastward), and (**d**) vertical profiles at the ROMS grid point nearest the SCMW of the temperature. Black line underlying subplot (**a**) indicates periods with high-quality IFCB data.

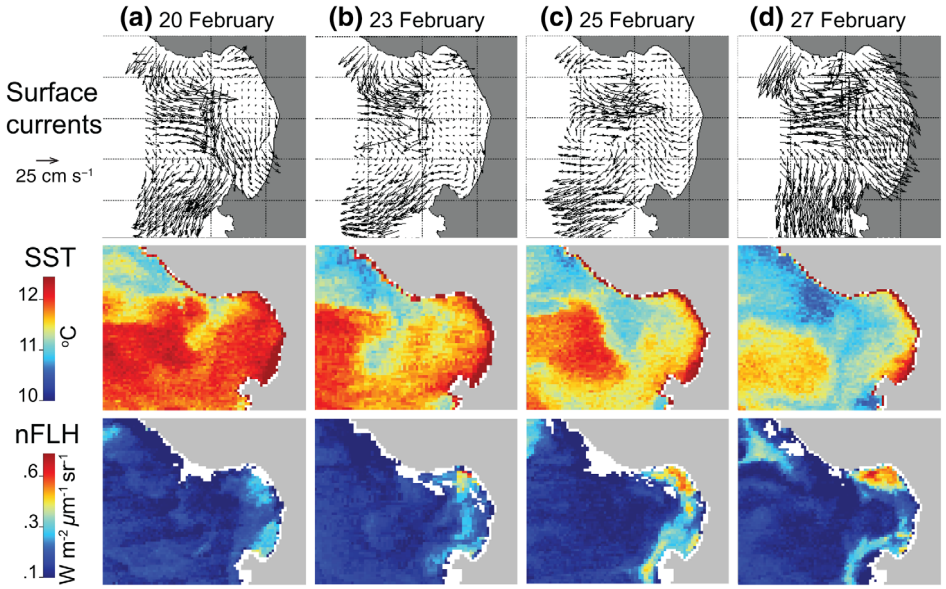

Fig. 6. Spatial description of bloom development in the northern Monterey Bay during an upwelling event in late February 2018. Top row shows HFr-derived surface currents, middle row shows satellite-observed SST, and bottom row shows satellite-observed chlorophyll nFLH.

and stratified waters resulted in a phytoplankton-specific carbon concentration of 35 μg L^{-1} (Fig. 4b) that was dominated by the dinoflagellates *Prorocentrum* spp. (max: 53 cells mL^{-1}), *A. sanguinea* (max: 52 cells mL^{-1}), and *Gymnodinium* spp. (max: 48 cells mL^{-1}) (Fig. 5a). A small upwelling event from 16 to 18 March advected the dinoflagellate bloom away from the SCMW (observed as ~ 1 cell mL^{-1}). During the second reversal/relaxation period (19–23 March), northwestward surface currents advected the bloom back to the SCMW, which was observed as a phytoplankton carbon biomass of 37 μg L^{-1} (Fig. 4a,b) that was dominated by *A. sanguinea* (max: 35 cells mL^{-1}), *Gymnodinium* spp. (max: 28 cells mL^{-1}), and *Prorocentrum* spp. (max: 24 cells mL^{-1}) (Fig. 5a). Dinoflagellate populations decreased markedly following the return of upwelling-favorable winds (Fig. 5b) and a large river discharge event on 21–23 March (Fig. 4d), which flushed the bay.

In May, intervals of regional upwelling wind reversals and relaxation produced a large dinoflagellate bloom and the highest phytoplankton-specific carbon biomass of 2018. Regional winds relaxed from 12 to 17 May (Fig. 5b), producing warmer SSTs and stratification (Fig. 5d). Cross-shore currents were predominantly poleward, which would have concentrated cells in the northern bay (Fig. 5c). These events resulted in maximum concentrations of 295 cells mL^{-1} of *A. sanguinea* and 143 cells mL^{-1} of *Prorocentrum* spp. (Fig. 5a), and a phytoplankton-specific carbon concentration of 87 μg L^{-1}. From 18 to 22 May, an upwelling event and southeastward surface currents moved the dinoflagellate bloom water mass away from the SCMW, resulting in cell concentrations close to 0 at the SCMW. As soon as the second relaxation period occurred (24–27 May), the surface currents became weakly northwestward and returned the bloom to the SCMW region. SSTs warmed and stratification increased once again (Fig. 5d), resulting in maximum *A. sanguinea* concentrations of 199 cells mL^{-1} (Fig. 5a). The return of upwelling-favorable winds on 28 May coincided with the bloom's demise. Strong upwelling from June through mid-July led to a diatom proliferation, especially the genus *Chaetoceros* (Fig. 4). Intermittent relaxation events during 24 June–05 July and 12–22 July resulted in dinoflagellate blooms dominated by the genus *Prorocentrum* (max: 375 cells mL^{-1}).

Upwelling weakened from mid-August through October and surface waters became increasingly warmer, stratified, and less turbulent (Fig. 4c). These conditions led to a dinoflagellate bloom that produced the second highest phytoplankton carbon concentration of 2018: 78 μg L^{-1} on 24 August (Fig. 4b). In contrast to the *A. sanguinea*-dominated blooms in March and May, the autumn biomass was dominated by the genera *Gymnodinium*, *Margalefidinium* (previously *Cochlodinium*; Gómez et al. 2017), and *Prorocentrum* (Fig. 4a). An unseasonally long upwelling period occurred from 17 October through 10 November and was followed by a series of regional wind relaxations/reversals and upwelling events lasting the duration of November (Fig. 4c). This return of upwelling-relaxation oscillations coincided with the return of higher *A. sanguinea* biomass, which attained a maximum cell concentration of 32 cells mL^{-1} on 16 November. Along with *A. sanguinea*, these conditions produced a population spike of the genera *Gymnodinium* (118 cells mL^{-1}) and *Margalefidinium* (90 cells mL^{-1}) and a phytoplankton-specific carbon concentration of 70 μg L^{-1} (Fig. 4a,b). This bloom was followed by rainfall events on 22–24 November, 29–30 November, and

17 December that may have flushed the bay (Fig. 4d), considerably reducing the total phytoplankton carbon concentrations to an average of 3 μg L^{-1} during December (Fig. 4b).

Discussion

The historically diatom-dominated phytoplankton assemblage of the northern Monterey Bay (e.g., Bolin and Abbot 1963; Garrison 1979) shifted to an anomalous dinoflagellate-dominated period twice in the last 18 years: 2004–2007 and 2017–2018. PLSR analysis demonstrated that both periods were linked to a negative NPGO and increased river discharge, but had different relationships to upwelling. Weakened upwelling was associated with the 2004–2007 dinoflagellate anomaly, which is consistent with the classical stratification-dinoflagellate bloom paradigm of Margalef's Mandala (Margalef 1978; Margalef et al. 1979). However, the 2017–2018 dinoflagellate anomaly occurred during a strong upwelling anomaly. High temporal resolution IFCB and satellite observations in 2018 provide evidence of dinoflagellate aggregations at upwelling fronts and onshore transport during relaxation, seeding the nearshore waters. Local winds and consecutive upwelling-relaxation cycles created a retentive circulation pattern, warmer SSTs, and stratification in the northern bay, which supported dinoflagellate bloom development. While we describe a local anomaly, there are implications for the larger CCS, which are discussed in the next section.

Nearshore blooms initiate in the transition from upwelling to relaxation

In 2018, the highest biomass dinoflagellate blooms in the northern Monterey Bay occurred following the transition from regional upwelling to relaxation in early-March, mid-May, late-August, and mid-November (Fig. 4). Both the timing of the appearance of dinoflagellate populations at the SCMW and their species composition suggest that upwelling convergent frontal zones may have served as "pelagic seed banks," as has been observed in other coastal upwelling systems (Pitcher et al. 1998, 2010; Smayda 2002*a*). Woodson et al. (2009) emphasized that the circulation within the Monterey Bay upwelling shadow near the front can provide a mechanism for nearshore retention and onshore transport of phytoplankton. By this mechanism, cells accumulate in frontal zones during active upwelling and then become entrained in weakened, across-shelf currents directed onshore during relaxation, a dispersion which seeds nearshore habitats and can lead to local blooms.

When cold, recently upwelling water enters the northern Monterey Bay, a thermal front develops where it encounters the warm, upwelling shadow. For example, an upwelling thermal front is apparent in SST satellite imagery and in a surface current convergence zone during late-February 2018 (Fig. 6). Despite sharp horizontal and vertical velocity gradients, dinoflagellates can aggregate and grow along fronts if their upward swimming velocity is sufficient to overcome downwelling at the convergence (Franks 1997; Pitcher et al. 1998; Ryan et al. 2009). In the initial days of a relaxation event, the incoming cells at the SCMW were dominated by *A. sanguinea*, *Ceratium* spp., *Margalefidinium* spp., and *Gymnodinium* spp. (Fig. 4a), which are life-form types IV, V, and VI (Smayda and Reynolds 2001; Smayda 2002*b*). Due to adaptations including strong swimming capability and chain formation, these dinoflagellate types are capable of withstanding turbulent vertical mixing and horizontal velocities and shear, and therefore surviving frontal zones, upwelling–relaxation habitats, and coastal currents (Smayda and Reynolds 2001; Smayda 2002*b*). During relaxation and reversal intervals, weakened across-shelf currents would have transported these frontal populations to the nearshore, where they were observed at SCMW (Fig. 5a). Future studies using autonomous underwater vehicles capable of sampling phytoplankton population at upwelling fronts and their trajectory toward the nearshore are needed to more conclusively test this hypothesized mechanism of bloom initiation.

The most dominant phytoplankton in 2018 was *A. sanguinea* (Fig. 4a)—a HAB species which has produced several massive blooms and associated seabird mortality events along the CCS in the past two decades (Cloern et al. 2005; Jessup et al. 2009; Du et al. 2011; White et al. 2014; Jones et al. 2017). *A. sanguinea* is detrimental to seabirds, abalone larvae and spat, and oysters (Woelke 1959; Cardwell et al. 1979; Botes et al. 2003; Jessup et al. 2009; Jones et al. 2017), but it was not linked to deleterious effects on local wildlife in 2018. *A. sanguinea* was likely able to maintain populations and outcompete other taxa in the strong upwelling conditions due to its biophysical tolerance to elevated shear and turbulence, as well as high growth rates (~ 1.13 divisions d^{-1}) (Smayda 2000; Matsubara et al. 2007; Kudela et al. 2010). Strong upwelling may also have enabled *A. sanguinea* to outgrow and "escape" parasitism by *Amoebophrya*, which is a known biological control on this species in Monterey Bay (Mazzillo et al. 2011).

Local winds enhance bloom retention

The northern Monterey Bay generally has a prolonged residence time and weak wind mixing, due to its sheltered position oceanographically and meteorologically. Water mass retention was further enhanced during the 2017–2018 dinoflagellate anomaly due to local winds blowing anomalously eastward and northward (Fig. 2, Supporting Information Fig. S3), while local alongshore surface currents (influenced by local and regional winds) shifted direction quasi-periodically (Fig. 5c). The combination of these conditions prevented the upwelling shadow water mass from being flushed from the bay (Woodson et al. 2009), and were likely responsible for anomalous warm and nitrate poor surface waters at the SCMW during this time period (Fig. 2). A warm, stratified, nutrient-depleted water mass in the upwelling shadow has been observed to function as a dinoflagellate bloom incubator in

many other instances (e.g., Rienecker et al. 2008; Ryan et al. 2008). Thus, when frontal dinoflagellate populations were transported into the upwelling shadow during relaxation events, they were retained and incubated.

The timing of the 2017–2018 dinoflagellate anomaly corresponds to local winds shifting to predominantly northward and eastward (Fig. 2). When local winds were used as the only explanatory variable in a 2012–2018 PLSR, the model could predict 33% of anomalous dinoflagellate chlorophyll annually and 54% in just January–May (Supporting Information Fig. S2). Unfortunately, the direction of local winds prior to 2012 cannot be examined due to no equivalent data sets, but similar wind anomalies during the 2004–2007 dinoflagellate anomaly are a compelling explanation. The connection between local winds and the frequency of upwelling-relaxation cycles also remains unexamined. Given the statistical importance of local wind forcing on dinoflagellate abundance and overlap with warm surface temperature and nitrate depletion anomalies, northward and eastward wind anomalies may be a proxy for an exceptionally retentive upwelling shadow water mass. Similarly, local wind forcing is the dominant control on nearshore temperature variability and circulation patterns in another central CCS embayment, San Luis Obispo Bay, where conditions act to increase local residence times and stratification, which could also create a bloom incubator (Walter et al. 2017).

A retentive upwelling shadow would also incubate diatom blooms, so how did dinoflagellates outcompete diatoms during mid-2017–2018? Vertical migration would have given dinoflagellates a competitive advantage in the low surface nutrients and strong upwelling conditions that characterized this period (Fig. 2). Dinoflagellates can access nutrients at depth via vertical swimming, which would have given them a significant advantage over diatom populations—notably the 2017–2018 dinoflagellate anomaly coincides with a low surface nitrate anomaly at SCMW (Fig. 2). Vertical migration to deeper layers with weaker currents would presumably have also helped dinoflagellates evade upwelling advection. During upwelling, the northern bay water mass is advected southward and the bay is flushed with upwelled water. In a modeling study, Shulman et al. (2012) showed that most dinoflagellates from the northern Monterey Bay avoided upwelling advection, while nonswimming phytoplankton, such as diatoms, were advected away. Most dinoflagellate taxa observed at SCMW in 2018 were capable of withstanding the turbulent vertical mixing associated with upwelling-relaxation cycles but of course, swimming behavior depends on many factors including physical conditions, light, prey pressure, and food availability (e.g., Smayda 2000).

Interannual drivers of dinoflagellate biomass

Both positive dinoflagellate anomalies in the past 18 years were associated with positive river discharge anomalies (Figs. 2, 3), likely due to physical changes in the nearshore water column. Drifter studies indicate that riverine and estuarine plumes in central Monterey Bay become entrained in the northward flowing, nearshore current and are transported to the northern bay (Fischer et al. 2014). Plume waters are rich in bacteria and cryptophytes, which could provide a food source for mixotrophic dinoflagellates (Jeong et al. 2005; Kudela et al. 2008), such as *A. sanguinea* which was dominant at the SCMW during the recent dinoflagellate anomaly. Inputs of low-density freshwater also enhances short-term stratification and nutrient supply from agricultural runoff (e.g., Kudela and Chavez 2004). The contribution from this plume and its transport northward may play an important role in fueling dinoflagellate blooms in the northern Monterey Bay (Fischer et al. 2014). River discharge has also been shown to be an important trigger for dinoflagellate blooms in other coastal systems due to increased stratification and nutrients (e.g., Carlsson et al. 1995; Hallegraeff et al. 1995; Weise et al. 2002).

A negative NPGO was also connected to the 2004–2007 and 2017–2018 dinoflagellate anomalies (Figs. 2, 3). The NPGO explains the dominant decadal fluctuations of salinity, nutrient upwelling, and Chl *a* in the Northeast Pacific region (Di Lorenzo et al. 2008, 2009). Numerical simulations reveal that a negative NPGO is associated with a delay in spring upwelling and weaker upwelling winds in the CCS, which are less efficient at uplifting nutrients, resulting in less productive planktonic ecosystems throughout the spring and summer (Chenillat et al. 2012). The resulting stratified and nutrient-depleted sea surface conditions would be expected to favor vertically swimming dinoflagellates over diatoms. The effects of a negative NPGO on phytoplankton travel up the food web and have been associated with population declines of plankton, finfish, and crustaceans along the CCS (Cloern et al. 2010; Sydeman and Thompson 2010).

Although the NPGO was in its negative phase during both dinoflagellate-dominated periods, its associated effect of weakened upwelling in the CCS (Chenillat et al. 2012) was only statistically important in the PLSR model predicting the 2004–2007 dinoflagellate anomaly (Figs. 2, 3). One possible explanation is that both MEI phases coincided with the 2004–2007 anomaly, whereas only a negative MEI coincided with the 2017–2018 anomaly. During a negative MEI, the California Current strengthens, upwelling intensity increases, SST decreases, and the mixed layer depth shoals, which typically results in increased surface nutrients and phytoplankton productivity (Barber and Chavez 1983; Behrenfeld et al. 2006). Given that anomalously strong upwelling characterized the Monterey Bay region in 2017–2018 (Fig. 2), the positive upwelling signal of a negative MEI seems to have overshadowed the opposing signal of a negative NPGO in the central CCS.

Future implications in the CCS

The link between northern Monterey Bay dinoflagellate abundance and the NPGO and regional upwelling can be used to contextualize potential ecosystem responses to future

changes in the CCS. Under anthropogenic climate change, stronger coupling is expected between the two dominant modes of North Pacific decadal variability, NPGO and the PDO, which will lead to more prolonged multiyear warm events with large spatial coverage over the Northeast Pacific (Joh and Di Lorenzo 2017; Liguori and Di Lorenzo 2018). A positive PDO was associated with increased dinoflagellate abundance off the Oregon coast (Du et al. 2015), although no relationship was found in this study. One possible explanation is that CCS upwelling variability is better correlated with the PDO north of 38°N (e.g., Oregon) and the NPGO south of 38°N (e.g., Monterey Bay) (Chhak and Di Lorenzo 2007; Di Lorenzo et al. 2008). Furthermore, over the past three decades, there has been an increase in the strength and variance of the NPGO (Sydeman et al. 2013), as well as its ecological significance to the north-central CCS (Cloern et al. 2010; Sydeman and Thompson 2010; Sydeman et al. 2013). This predicted increase in stratified waters with lower surface nutrients in the CCS and a strongly negative NPGO would presumably favor dinoflagellate proliferation (including HAB species).

Climate warming is projected to increase the strength of upwelling-favorable winds in most eastern boundary upwelling systems with some latitudinal and regional variation (Bakun 1990; Sydeman et al. 2014; Wang et al. 2015). The strength of upwelling winds is expected to increase in much of the CCS, including the central coast (García-Reyes and Largier 2010). This would produce an earlier onset of the upwelling season and intensification of peak upwelling season winds, such that in some cases, they could be stronger than the optimal value for phytoplankton in the nearshore. If future upwelling wind intensification scenarios in the central CCS and local forcings generate conditions similar to Monterey Bay in 2017–2018, this could potentially lead to a proliferation of dinoflagellates. On the other hand, there are more examples of weakened upwelling producing ideal conditions for dinoflagellate blooms, including 2004–2007 in Monterey Bay, so increased upwelling could also lead to a reduction in dinoflagellate abundance. To examine if changes in North Pacific decadal variability and coastal upwelling will ultimately lead to more "ages of dinoflagellates," there is a continued need for long-term phytoplankton and environmental time series and associated studies throughout the CCS.

Conclusion

Within coastal upwelling systems, local features and forcings have the ability to amplify or reduce the effects of regional and basin-scale forcings (e.g., the delivery of nutrients and water column stability) and alter phytoplankton abundance and composition at a local scale (Kudela et al. 2005; Ryan et al. 2008, 2014; Walter et al. 2017). This study demonstrates the necessity of investigating both fine-scale shifts in phytoplankton and environmental conditions to understand local dynamics, as well as the relative abundance of phytoplankton over interannual timescales to assess the impact of regional and basin-scale climate events on local ecosystems. This methodology allowed us to discover similarities and differences between the conditions producing two anomalous dinoflagellate-dominated periods in Monterey Bay over the past 18 years, including an unexpected interaction between regional upwelling cycles and local wind forcing in the recent period. Examining deviations from canonical phytoplankton patterns in these types of studies is increasingly important because they can provide insights into how different phytoplankton groups and ecosystems may respond to anthropogenic climate change in the coming century, and how local forcing can override this secular forcing. Fortunately, new sampling technologies (e.g., IFCB) and lengthening observational time series have made examining this complex interplay between short- and long-term forcings more possible now than ever before.

References

Abdi, H. 2010. Partial least squares regression and projection on latent structure regression (PLS regression). WIREs Comp. Stat. **2**: 97–106. doi:10.1002/wics.51

Bakun, A. 1973. Coastal upwelling indices, west coast of North America, 1946–71, p. 1–103. NOAA Tech. Report, U.S. Department of Commerce, Seattle, WA, NMFS SSRF-671.

Bakun, A. 1990. Global climate change and intensification of coastal ocean upwelling. Science **247**: 198–201. doi:10.3354/meps274235

Barber, R. T., and F. P. Chavez. 1983. Biological consequences of El Niño. Science **222**: 1203–1210. doi:10.1126/science.222.4629.1203

Behrenfeld, M. J., and others. 2006. Climate-driven trends in contemporary ocean productivity. Nature **444**: 752–755. doi:10.1038/nature05317

Bolin, R. L., and D. P. Abbot. 1963. Studies on the marine climate and phytoplankton of the central coastal area of California, 1954–1960. CalCOFI Rep. **9**: 23–45.

Botes, L., A. J. Smit, and P. A. Cook. 2003. The potential threat of algal blooms to the abalone (*Haliotis midae*) mariculture industry situated around the South African coast. Harmful Algae **2**: 247–259. doi:10.1016/S1568-9883(03)00044-1

Breiman, L. 2001. Random forests. Mach. Learn. **45**: 5–32.

Cardwell, R. D., S. Olsen, M. I. Carr, and E. W. Sanborn. 1979. Causes of oyster larvae mortality in South Puget Sound. NOAA Tech. Memo, Washington Department of Fisheries, Salmon Research and Development, Brinnan, Washington, ERL MESA-39.

Carlsson, P., E. Graneli, P. Tester, and L. Boni. 1995. Influences of riverine humic substances on bacteria, protozoa, phytoplankton, and copepods in a coastal plankton community. Mar. Ecol. Prog. Ser. **127**: 213–221. doi:10.3354/meps127213

Carrascal, L. M., I. Galván, and O. Gordo. 2009. Partial least squares regression as an alternative to current regression methods used in ecology. Oikos **118**: 681–690. doi:10.1111/j.1600-0706.2008.16881.x

Chavez, F. P. 2006. Seeing the future in the stratified sea, p. 16–18. *In* Monterey Bay Aquarium Research Institute 2006 annual report. Monterey Bay Aquarium Research Institute, Moss Landing, CA.

Chenillat, F., P. Riviére, X. Capet, E. Di Lorenzo, and B. Blanke. 2012. North Pacific Gyre Oscillation modulates seasonal timing and ecosystem functioning in the California Current upwelling system. Geophys. Res. Lett. **39**: 1–6. doi:10.1029/2011GL049966

Chhak, K., and E. Di Lorenzo. 2007. Decadal variations in the California Current upwelling cells. Geophys. Res. Lett. **34**: 1–6. doi:10.1029/2007GL030203

Cloern, J. E. 1996. Phytoplankton bloom dynamics in coastal ecosystems: A review with some general lessons from sustained investigation of San Francisco Bay, California. Rev. Geophys. **34**: 127–168. doi:10.1029/96RG00986

Cloern, J. E., T. S. Schraga, C. B. Lopez, N. Knowles, R. Grover Labiosa, and R. Dugdale. 2005. Climate anomalies generate an exceptional dinoflagellate bloom in San Francisco Bay. Geophys. Res. Lett. **32**: 1–5. doi:10.1029/2005GL023321

Cloern, J. E., and others. 2010. Biological communities in San Francisco Bay track large-scale climate forcing over the North Pacific. Geophys. Res. Lett. **37**: 1–6. doi:10.1029/2010GL044774

Curtiss, C. C., G. W. Langlois, L. B. Busse, F. Mazzillo, and M. W. Silver. 2008. The emergence of *Cochlodinium* along the California Coast (USA). Harmful Algae **7**: 337–346. doi:10.1016/j.hal.2007.12.012

Di Lorenzo, E., and others. 2008. North Pacific Gyre Oscillation links ocean climate and ecosystem change. Geophys. Res. Lett. **35**: 2–7. doi:10.1029/2007GL032838

Di Lorenzo, E., and others. 2009. Nutrient and salinity decadal variations in the central and eastern North Pacific. Geophys. Res. Lett. **36**: 2003–2008. doi:10.1029/2009GL038261

Du, X., W. Peterson, A. McCulloch, and G. Liu. 2011. An unusual bloom of the dinoflagellate *Akashiwo sanguinea* off the central Oregon, USA, coast in autumn 2009. Harmful Algae **10**: 784–793. doi:10.1016/j.hal.2011.06.011

Du, X., W. Peterson, and L. O'Higgins. 2015. Interannual variations in phytoplankton community structure in the northern California Current during the upwelling seasons of 2001–2010. Mar. Ecol. Prog. Ser. **519**: 75–87. doi:10.3354/meps11097

Figueiras, F. G., and A. F. Ríos. 1993. Phytoplankton succession, red tides, and the hydrographic regime in the Rías Bajas of Galicia, p. 239–244. *In* T. J. Smayda and Y. Shimizu [eds.], Toxic phytoplankton blooms in the sea. Elsevier.

Fischer, A. M., J. P. Ryan, C. Levesque, and N. Welschmeyer. 2014. Characterizing estuarine plume discharge into the coastal ocean using fatty acid biomarkers and pigment analysis. Mar. Environ. Res. **99**: 106–116. doi:10.1016/j.marenvres.2014.04.006

Franks, P. J. S. 1997. Spatial patterns in dense algal blooms. Limnol. Oceanogr. **42**: 1297–1305. doi:10.4319/lo.1997.42.5_part_2.1297

García-Reyes, M., and J. Largier. 2010. Observations of increased wind-driven coastal upwelling off Central California. J. Geophys. Res. Oceans **115**: 1–8. doi:10.1029/2009JC005576

García-Reyes, M., and J. L. Largier. 2012. Seasonality of coastal upwelling off central and northern California: New insights, including temporal and spatial variability. J. Geophys. Res. Oceans **117**: 1–17. doi:10.1029/2011JC007629

Garrison, D. L. 1979. Monterey Bay phytoplankton I. Seasonal cycles of phytoplankton assemblages. J. Plankton Res. **1**: 241–265. doi:10.1093/plankt/1.3.241

Gómez, F., M. L. Richlen, and D. M. Anderson. 2017. Molecular characterization and morphology of *Cochlodinium strangulatum*, the type species of *Cochlodinium*, and *Margalefidinium* gen. nov. for *C. polykrikoides* and allied species (Gymnodiniales, Dinophyceae). Harmful Algae **63**: 32–44. doi:10.1016/j.hal.2017.01.008

Graham, W. M., and J. L. Largier. 1997. Upwelling shadows as nearshore retention sites: The example of northern Monterey Bay. Cont. Shelf Res. **17**: 509–532. doi:10.1016/S0278-4343(96)00045-3

Hallegraeff, G. M., M. A. Mccausland, and R. K. Brown. 1995. Early warning of toxic dinoflagellate blooms of *Gymnodinium catenatum* in southern Tasmanian waters. J. Plankton Res. **17**: 1163–1176. doi:10.1093/plankt/17.6.1163

Hoell, A., M. Hoerling, J. Eischeid, K. Wolter, R. Dole, J. Perlwitz, T. Xu, and L. Cheng. 2015. Does El Niño intensity matter for California precipitation? Geophys. Res. Lett. **43**: 819–825. doi:10.1002/2015GL067102

Jeong, H. J., D. Y. Yeong, Y. P. Y. S. Jae, Y. P. Y. S. Jae, T. K. Seong, H. L. Seung, Y. K. Kwang, and H. Y. Won. 2005. Feeding by phototrophic red-tide dinoflagellates: Five species newly revealed and six species previously known to be mixotrophic. Aquat. Microb. Ecol. **40**: 133–150. doi:10.3354/ame040133

Jessup, D. A., and others. 2009. Mass stranding of marine birds caused by a surfactant-producing red tide. PLoS One **4**: e4550. doi:10.1371/journal.pone.0004550

Jester, R. J., K. A. Baugh, and K. A. Lefebvre. 2009*a*. Presence of *Alexandrium catenella* and paralytic shellfish toxins in finfish, shellfish and rock crabs in Monterey Bay, California, USA. Mar. Biol. **156**: 493–504. doi:10.1007/s00227-008-1103-z

Jester, R. J., K. Lefebvre, G. Langlois, V. Vigilant, K. Baugh, and M. W. Silver. 2009*b*. A shift in the dominant toxin-producing algal species in central California alters phycotoxins in food webs. Harmful Algae **8**: 291–298. doi:10.1016/j.hal.2008.07.001

Joh, Y., and E. Di Lorenzo. 2017. Increasing coupling between NPGO and PDO leads to prolonged marine heatwaves in the Northeast Pacific. Geophys. Res. Lett. **44**: 11663–11671. doi:10.1002/2017GL075930

Jones, T., and others. 2017. Mass mortality of marine birds in the Northeast Pacific caused by *Akashiwo sanguinea*. Mar. Ecol. Prog. Ser. **579**: 111–127. doi:10.3354/meps12253

Kudela, R. M., and F. P. Chavez. 2004. The impact of coastal runoff on ocean color during an El Niño year in Central California. Deep-Sea Res. Part II Top. Stud. Oceanogr. **51**: 1173–1185. doi:10.1016/j.dsr2.2004.04.002

Kudela, R. M., G. Pitcher, T. Probyn, F. Figueiras, T. Moita, and V. Trainer. 2005. Harmful algal blooms upwelling systems. Oceanography **18**: 184–197. doi:10.5670/oceanog.2005.53

Kudela, R. M., J. Q. Lane, and W. P. Cochlan. 2008. The potential role of anthropogenically derived nitrogen in the growth of harmful algae in California, USA. Harmful Algae **8**: 103–110. doi:10.1016/j.hal.2008.08.019

Kudela, R. M., S. Seeyave, and W. P. Cochlan. 2010. The role of nutrients in regulation and promotion of harmful algal blooms in upwelling systems. Prog. Oceanogr. **85**: 122–135. doi:10.1016/j.pocean.2010.02.008

Lane, J. Q., P. T. Raimondi, and R. M. Kudela. 2009. Development of a logistic regression model for the prediction of toxigenic *Pseudo-nitzschia* blooms in Monterey Bay, California. Mar. Ecol. Prog. Ser. **383**: 37–51. doi:10.3354/meps07999

Liguori, G., and E. Di Lorenzo. 2018. Meridional modes and increasing Pacific decadal variability under anthropogenic forcing. Geophys. Res. Lett. **45**: 983–991. doi:10.1002/2017GL076548

Litz, M. N. C., R. D. Brodeur, R. L. Emmett, S. S. Heppell, R. S. Rasmussen, L. O'Higgins, and M. S. Morris. 2010. Effects of variable oceanographic conditions on forage fish lipid content and fatty acid composition in the northern California Current. Mar. Ecol. Prog. Ser. **405**: 71–85. doi:10.3354/meps08479

Margalef, R. 1978. Life-forms of phytoplankton as survival alternatives in an unstable environment. Oceanol. Acta **1**: 493–509.

Margalef, R., M. Estrada, and D. Blasco. 1979. Functional morphology of organisms involved in red tides, as adapted to decaying turbulence, p. 89–94. *In* D. L. Taylor and H. H. Seliger [eds.], Toxic dinoflagellate blooms. Elsevier.

Matsubara, T., S. Nagasoe, Y. Yamasaki, T. Shikata, Y. Shimasaki, Y. Oshima, and T. Honjo. 2007. Effects of temperature, salinity, and irradiance on the growth of the dinoflagellate *Akashiwo sanguinea*. J. Exp. Mar. Biol. Ecol. **342**: 226–230. doi:10.1016/j.jembe.2006.09.013

Mazzillo, F. F. M., J. P. Ryan, and M. W. Silver. 2011. Parasitism as a biological control agent of dinoflagellate blooms in the California Current System. Harmful Algae **10**: 763–773. doi:10.1016/j.hal.2011.06.009

Menden-Deuer, S., and E. J. Lessard. 2000. Carbon to volume relationships for dinoflagellates, diatoms, and other protist plankton. Limnol. Oceanogr. **45**: 569–579. doi:10.4319/lo.2000.45.3.0569

Moberg, E. A., and H. M. Sosik. 2012. Distance maps to estimate cell volume from two-dimensional plankton images. Limnol. Oceanogr.: Methods **10**: 278–288. doi:10.4319/lom.2012.10.278

Olson, R. J., and H. M. Sosik. 2007. A submersible imaging-in-flow instrument to analyze nano-and microplankton: Imaging FlowCytobot. Limnol. Oceanogr.: Methods **5**: 195–203. doi:10.4319/lom.2007.5.195

Pennington, J. T., and F. P. Chavez. 2000. Seasonal fluctuations of temperature, salinity, nitrate, chlorophyll and primary production at station H3/M1 over 1989–1996 in Monterey Bay, California. Deep-Sea Res. Part II Top. Stud. Oceanogr. **47**: 947–973. doi:10.1016/S0967-0645(99)00132-0

Pennington, J. T., and F. P. Chavez. 2017. Decade-scale oceanographic fluctuation in Monterey Bay, California, 1989–2011. Deep-Sea Res. Part II Top. Stud. Oceanogr. **151**: 4–15. doi:10.1016/j.dsr2.2017.07.005

Peterson, W. T., and F. B. Schwing. 2003. A new climate regime in northeast pacific ecosystems. Geophys. Res. Lett. **30**: 1–4. doi:10.1029/2003GL017528

Peterson, W. T., and others. 2006. The state of the California Current, 2005–2006: Warm in the north, cool in the south. CalCOFI Rep. **47**: 30–75.

Pitcher, G. C., A. J. Boyd, D. A. Horstman, and B. A. Mitchell-Innes. 1998. Subsurface dinoflagellate populations, frontal blooms and the formation of red tide in the southern Benguela upwelling system. Mar. Ecol. Prog. Ser. **172**: 253–264. doi:10.3354/meps172253

Pitcher, G. C., F. G. Figueiras, B. M. Hickey, and M. T. Moita. 2010. The physical oceanography of upwelling systems and the development of harmful algal blooms. Prog. Oceanogr. **85**: 5–32. doi:10.1016/j.pocean.2010.02.002

Platt, T., C. Fuentes-Yaco, and K. T. Frank. 2003. Spring algal bloom and larval fish survival. Nature **423**: 398–399.

Rienecker, E., J. Ryan, M. Blum, C. Dietz, L. Coletti, R. Marin, and W. Paul Bissett. 2008. Mapping phytoplankton in situ using a laser-scattering sensor. Limnol. Oceanogr.: Methods **6**: 153–161. doi:10.4319/lom.2008.6.153

Rosenfeld, L. K., F. B. Schwing, N. Garfield, and D. E. Tracy. 1994. Bifurcated flow from an upwelling center: A cold water source for Monterey Bay. Cont. Shelf Res. **14**: 931–964. doi:10.1016/0278-4343(94)90058-2

Ryan, J., and others. 2011. Harmful phytoplankton ecology studies using an autonomous molecular analytical and ocean observing network. Limnol. Oceanogr. **56**: 1255–1272. doi:10.4319/lo.2011.56.4.1255

Ryan, J. P., and others. 2008. A coastal ocean extreme bloom incubator. Geophys. Res. Lett. **35**: 4–8. doi:10.1029/2008GL034081

Ryan, J. P., A. M. Fischer, R. M. Kudela, J. F. R. Gower, S. A. King, R. Marin, and F. P. Chavez. 2009. Influences of upwelling and downwelling winds on red tide bloom dynamics in Monterey Bay, California. Cont. Shelf Res. **29**: 785–795. doi:10.1016/j.csr.2008.11.006

Ryan, J. P., and others. 2014. Boundary influences on HAB phytoplankton ecology in a stratification-enhanced upwelling shadow. Deep-Sea Res. Part II Top. Stud. Oceanogr. **101**: 63–79. doi:10.1016/j.dsr2.2013.01.017

Ryther, J. H. 1969. Photosynthesis and fish production in the sea. Science **166**: 72–76.

Schulien, J. A., M. B. Peacock, K. Hayashi, P. Raimondi, and R. M. Kudela. 2017. Phytoplankton and microbial abundance and bloom dynamics in the upwelling shadow of Monterey Bay, California, from 2006 to 2013. Mar. Ecol. Prog. Ser. **572**: 43–56. doi:10.3354/meps12142

Shulman, I., B. Penta, M. A. Moline, S. H. D. Haddock, S. Anderson, M. J. Oliver, and P. Sakalaukus. 2012. Can vertical migrations of dinoflagellates explain observed bioluminescence patterns during an upwelling event in Monterey Bay, California? J. Geophys. Res. Oceans **117**: 1–10. doi:10.1029/2011JC007480

Singh, A., A. R. Jakubowski, I. Chidister, and P. A. Townsend. 2013. A MODIS approach to predicting stream water quality in Wisconsin. Remote Sens. Environ. **128**: 74–86. doi:10.1016/j.rse.2012.10.001

Smayda, T. J. 2000. Ecological features of harmful algal blooms in coastal upwelling ecosystems. S. Afr. J. Mar. Sci. **22**: 219–253. doi:10.2989/025776100784125816

Smayda, T. J. 2002*a*. Turbulence, watermass stratification and harmful algal blooms: An alternative view and frontal zones as "pelagic seed banks". Harmful Algae **1**: 95–112. doi:10.1016/S1568-9883(02)00010-0

Smayda, T. J. 2002*b*. Adaptive ecology, growth strategies and the global bloom expansion of dinoflagellates. J. Oceanogr. **58**: 281–294. doi:10.1023/A:1015861725470

Smayda, T. J., and C. S. Reynolds. 2001. Community assembly in marine phytoplankton: Application of recent models to harmful dinoflagellate blooms. J. Plankton Res. **23**: 447–461. doi:10.1093/plankt/23.5.447

Sommer, U. 2002. Competition and coexistence in plankton communities, p. 79–108. *In* E. Sommer and B. Worm [eds.], Competition and coexistence. Springer.

Sosik, H. M., and R. J. Olson. 2007. Automated taxonomic classification of phytoplankton sampled with imaging-in-flow cytometry. Limnol. Oceanogr.: Methods **5**: 204–216. doi:10.4319/lom.2007.5.204

Stineman, R. W. 1980. A consistently well behaved method of interpolation. Creat. Comput. **6**: 54–57.

Sydeman, W. J., and others. 2006. Planktivorous auklet *Ptychoramphus aleuticus* responses to ocean climate, 2005: Unusual atmospheric blocking? Geophys. Res. Lett. **33**: 1–5. doi:10.1029/2006GL026736

Sydeman, W. J., and S. A. Thompson. 2010. The California Current Integrated Ecosystem Assessment (IEA), module II: Trends and variability in climate-ecosystem state, p. 1–59. NOAA Tech. Rep. NMFS SWFSC Environ. Res. Div.

Sydeman, W. J., J. A. Santora, S. A. Thompson, B. Marinovic, and E. Di Lorenzo. 2013. Increasing variance in North Pacific climate relates to unprecedented ecosystem variability off California. Glob. Chang. Biol. **19**: 1662–1675. doi:10.1111/gcb.12165

Sydeman, W. J., M. García-Reyes, D. S. Schoeman, R. R. Rykaczewski, S. A. Thompson, B. A. Black, and S. J. Bograd. 2014. Climate change and wind intensification in coastal upwelling ecosystems. Science **345**: 77–80. doi:10.1126/science.1251635

Taylor, A. G., M. R. Landry, K. E. Selph, and J. J. Wokuluk. 2015. Temporal and spatial patterns of microbial community biomass and composition in the Southern California Current Ecosystem. Deep-Sea Res. Part II Top. Stud. Oceanogr. **112**: 117–128. doi:10.1016/j.dsr2.2014.02.006

Venrick, E. L. 2012. Phytoplankton in the California Current system off southern California: Changes in a changing environment. Prog. Oceanogr. **104**: 46–58. doi:10.1016/j.pocean.2012.05.005

Walter, R. K., E. C. Reid, K. A. Davis, K. J. Armenta, K. Merhoff, and N. J. Nidzieko. 2017. Local diurnal wind-driven variability and upwelling in a small coastal embayment. J. Geophys. Res. Oceans **122**: 955–972.

Wang, D., T. C. Gouhier, B. A. Menge, and A. R. Ganguly. 2015. Intensification and spatial homogenization of coastal upwelling under climate change. Nature **518**: 390–394. doi:10.1038/nature14235

Weise, A. M., and others. 2002. The link between precipitation, river runoff, and blooms of the toxic dinoflagellate *Alexandrium tamarense* in the St. Lawrence. Can. J. Fish. Aquat. Sci. **473**: 464–473. doi:10.1139/F02-024

Weise, M. J., D. P. Costa, and R. M. Kudela. 2006. Movement and diving behavior of male California sea lion (*Zalophus californianus*) during anomalous oceanographic conditions of 2005 compared to those of 2004. Geophys. Res. Lett. **33**: L22S10. doi:10.1029/2006GL027113

Welschmeyer, N. A. 1994. Fluorometric analysis of chlorophyll *a* in the presence of chlorophyll *b* and pheopigments. Limnol. Oceanogr. **39**: 1985–1992. doi:10.4319/lo.1994.39.8.1985

White, A. E., and others. 2014. Large-scale bloom of *Akashiwo sanguinea* in the Northern California current system in 2009. Harmful Algae **37**: 38–46. doi:10.1016/j.hal.2014.05.004

Woelke, C. E. 1959. Pacific oyster *Crassostrea gigas* mortalities with notes on common oyster predators in Washington waters. Proc. Natl. Shellfish. Assoc. **50**: 53–66.

Wolter, K., and M. S. Timlin. 2011. El Niño/Southern Oscillation behaviour since 1871 as diagnosed in an extended multivariate ENSO index (MEI.ext). Int. J. Climatol. **31**: 1074–1087. doi:10.1002/joc.2336

Woodson, C. B., L. Washburn, J. A. Barth, D. J. Hoover, A. R. Kirincich, M. A. McManus, J. P. Ryan, and J. Tyburczy. 2009. Northern Monterey Bay upwelling shadow front: Observations of a coastally and surface-trapped buoyant

plume. J. Geophys. Res. Oceans **114**: 1–15. doi:10.1029/2009JC005623

Acknowledgments

Special thanks to Sabrina Garcia, Emily Lancaster, Cristian Garces, Tina, and other staff and student members of R.M. Kudela's laboratory for assistance in sample collection and processing, to Ivory Engstrom, Matthew Bach, and Vinnie Ferreira for fielding IFCB support phone calls and emails, and to the staff at the Santa Cruz Municipal Wharf for assistance with IFCB deployments and retrievals. This work was supported by NOAA through grants from the Marine Sensors Transitions program (NA14NOS0120148), the Central and Northern California Ocean Observing System (CeNCOOS) through the Integrated Ocean Observing System (NA16NOS0120021), and the Saltonstall-Kennedy program (NA16NMF4270263) to R.M.K. Additional support was provided through a California Sea Grant Delta Science Postdoctoral Fellowship to A.D.F. (SEAAF18/182GEA/416723/440000).

Conflict of Interest

None declared.

Submitted 04 October 2019
Revised 24 January 2020
Accepted 03 February 2020

Associate editor: Susanne Menden-Deuer